Magnetic and ferroelectric properties of Zn and Mn co-doped $BaTiO_3$*

Sangram Keshari Das and Binod Kumar Roul†

Institute of Materials Science, Planetarium Building, Acharaya Vihar, Bhubaneswar-751013, Odisha, India

(Received 26 October 2014; revised manuscript received 7 January 2015; published online 10 April 2015)

This paper reports an approach to obtaining multiferroic properties in co-doped (Zn:Mn) $BaTiO_3$ near room temperature. Interestingly, an unusual magnetic hysteresis loop is observed in the co-doped compositions in which the central portion of the loop is squeezed. However, in the composition $Ba_{0.9}Zn_{0.1}Ti_{0.9}Mn_{0.1}O_3$, a broad magnetic hysteresis loop is observed. Such a magnetic effect is attributed to the coexistence of antiferromagnetic and ferromagnetic exchange interactions in the system. The observation of the above type of magnetic properties is likely to be due to the presence of exchange interactions between Mn ions. A lossy-type of ferroelectric hysteresis loop is also observed in co-doped ceramic compositions near room temperature.

Keywords: ferroelectrics, ceramic, ferromagnetic

PACS: 77.84.−s, 81.05.Mh, 76.50.+g **DOI:** 10.1088/1674-1056/24/6/067702

1. Introduction

The demand for miniaturization of devices during the 21st century has motivated research activities in multifunctional materials in which specific desirable electronic, magnetic, optical, thermal, or other properties are incorporated to satisfy previously unattainable performances.[1] Multifunctional materials are vital in emerging technological fronts and they also greatly reduce different material consumptions in multiple material component devices. These types of materials are designed to meet stringent requirements by tailoring different desirable properties. In this direction, coupling of different properties in a single material plays a vital role especially in electronic, spintronics, and photonic devices. Enhancement in coupling between magnetic and ferroelectric properties within a single phase material will find applications in the emerging field of multiferroics and spintronics. Magneto–electric multiferroics, in which ferromagnetism and ferroelectricity coexist in a single phase, has been becoming more and more attractive in recent years because of potential applications in multiple state memory elements, magnetic valve, filtering device, sensors, etc.[2] In magnetic ferroelectrics, magnetism is associated with spin degrees of freedom and ferroelectric response depends on charge degrees of freedom.[3] Crystalline compound in which magnetism and electric polarization coexist is quite rare in nature, particularly at room temperature and above.[3]

To circumvent this limitation, different approaches have been undertaken to address the issue. One of the proven approaches is to tailor existing known ABO_3-type ferroelectric materials by doping magnetic ions.[3–5] Barium titanate ($BaTiO_3$) is one of the ABO_3-type ferroelectric materials in which new properties especially the magnetic property can be induced because it is chemically and mechanically very stable.[6–8]

In order to improve the functional properties of $BaTiO_3$ (BTO), different dopants have been substituted for Ba^{2+} or Ti^{4+} of BTO.[5,10] BTO has been proven both theoretically and experimentally to be multiferroic by doping or synthesis on a nanoscale.[11–16] Theoretical calculation of Nakayama and Katayama–Yoshida has predicted ferromagnetic behavior in BTO by carrier doping.[13] The magnetic properties are also observed experimentally in Co, Mn, Cr, and Fe-doped BTO thin films and nanoparticles.[15] Room temperature ferromagnetic order has also been observed by Dang *et al.* in $BaTi_{1-x}Fe_xO_3$, with $x = 0.02$–0.06 and revealed that ferromagnetism depends strongly on the concentration of Fe ion impurities.[10]

Although transition metal (TM) doped BTO is a multifunctional material with potential applications in the emerging field of spintronics, the understanding of the origin of observed magnetism is still incomplete. Based on our preliminary experimental findings,[12] in the present paper a deep study is carried out to understand the basic mechanism involved in the occurrence of magnetism in this well studied material. We observe an unusual magnetic hysteresis loop with the squeezing of the central portion of the loop for all co-doped compositions. In addition to this, we also observe room temperature ferroelectric properties in all co-doped ceramic compositions.

*Author S. K. Das supported financially by CSIR, New Delhi (Grant No. 09/750 (0005)/2009-EMR-I).

†Corresponding author. E-mail: ims@iopb.res.in

© 2015 Chinese Physical Society and IOP Publishing Ltd

2. Experimental procedures

Polycrystalline samples of $Ba_{0.96}Zn_{0.04}Ti_{0.96}Mn_{0.04}O_3$, and $Ba_{0.9}Zn_{0.1}Ti_{0.9}Mn_{0.1}O_3$ were prepared by the conventional solid state reaction technique. High-purity (99.99%) $BaCO_3$, TiO_2, MnO, and ZnO powders were taken to have stoichiometric quantities according to the formula BTO $Ba_{0.96}Zn_{0.04}Ti_{0.96}Mn_{0.04}O_3$ and $Ba_{0.9}Zn_{0.1}Ti_{0.9}Mn_{0.1}O_3$, and mixed thoroughly by using agate mortar and pestle mixed powders were calcined in air at 950 °C for 24 h. Calcined powders were pressed into pellets and pellets were sintered at 1300 °C for 5 h.

Sintered samples were characterized by different techniques. Structural characterizations of sintered pellets were carried out by x-ray diffraction (XRD) using a Bruker (D8) powder diffractometer (Cu Kα1 = 1.5406 Å). XRD data refinements were done using the Full Prof software package. Optical properties were investigated by a micro-Raman spectrophotometer (RENI SHAW in Via Raman Microscope) with a 514-cm^{-1} laser line as an excitation source. Energy dispersive x-ray spectroscopy (EDS) was used to detect the elemental compositions of our sample using the Oxford EDS Detector. Magnetic measurements were done using VSM (Lakeshore, model no. 7410). Ferroelectric characterizations were carried out with ferroelectric loop tracer (Precision Premier-II, Radiant). Chemical bonding analyses of sintered pellets were performed using XPS (VG system with a base pressure of 1×10^{-10} Torr, 1 Torr = 1.33322×10^2 Pa). Microprocessor controlled programmable LCR meter bridge (Quadtech, USA) was used for dielectric study. The resistivity of samples is measured using Keithley's model 6517B electrometer.

3. Results and discussion

Structural characteristics of sintered samples are investigated by an x-ray diffraction technique. XRD patterns of BTO, $Ba_{0.96}Zn_{0.04}Ti_{0.96}Mn_{0.04}O_3$, and $Ba_{0.9}Zn_{0.1}Ti_{0.9}Mn_{0.1}O_3$ ceramics are shown in Fig. 1. The XRD peaks are indexed using our search test program.[17] $BaTiO_3$ (BTO) is identified as being in tetragonal phase (JCPDS file no. 83-1880) and $Ba_{0.9}Zn_{0.1}Ti_{0.9}Mn_{0.1}O_3$ is identified as being in hexagonal phase (JCPDS file no. 76-0738). However, in the composition $Ba_{0.96}Zn_{0.04}Ti_{0.96}Mn_{0.04}O_3$, peaks related to the tetragonal and hexagonal phase of BTO are seen. Figure 2 shows the XRD refinements[12] of BTO and $Ba_{0.9}Zn_{0.1}Ti_{0.9}Mn_{0.1}O_3$. The R-factors for BTO are $R_{wp} = 2.7\%$, $R_p = 2.6\%$, and $R_{exp} = 2.2\%$. The R-factors for $Ba_{0.9}Zn_{0.1}Ti_{0.9}Mn_{0.1}O_3$ are $R_{wp} = 2.8\%$, $R_p = 2.5\%$, and $R_{exp} = 2.1\%$. The refinement results reveal that lattice parameters of BTO are $a = b = 3.996$ Å, $c = 4.021$ Å, and $\alpha = \beta = \gamma = 90°$ with space group $p4mm$ and lattice parameters of $Ba_{0.9}Zn_{0.1}Ti_{0.9}Mn_{0.1}O_3$ are $a = b = 5.719$ Å, $c = 13.959$ Å, and $\alpha = \beta = 90°$ and $\gamma = 120°$ with space group $P6_3/mmc$.

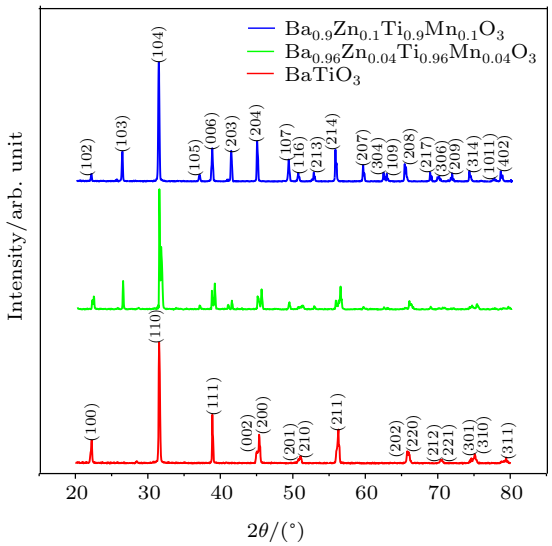


Fig. 1. (color online) The x-ray diffraction (XRD) patterns of $BaTiO_3$, $Ba_{0.96}Zn_{0.04}Ti_{0.96}Mn_{0.04}O_3$, and $Ba_{0.9}Zn_{0.1}Ti_{0.9}Mn_{0.1}O_3$.

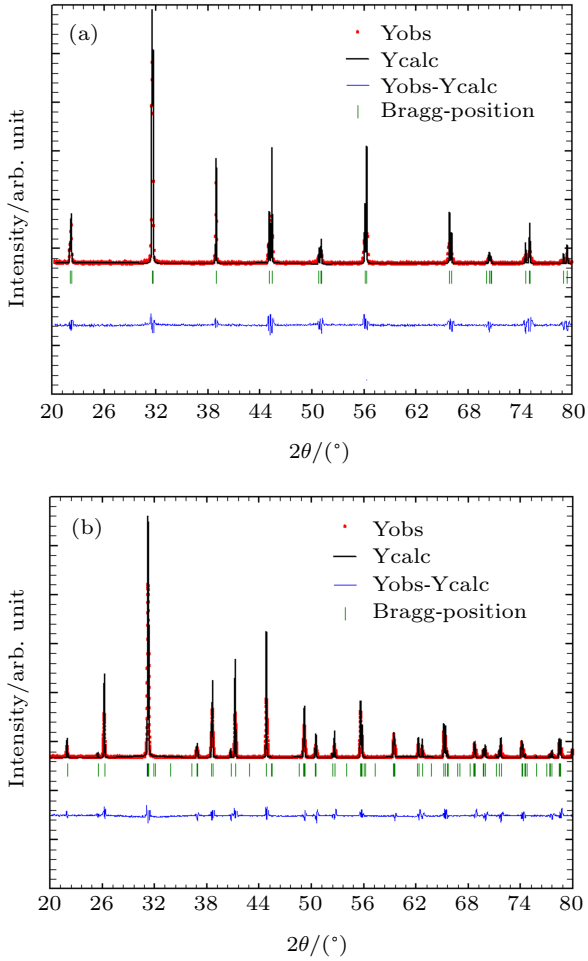


Fig. 2. (color online) The Rietveld refinements of (a) $BaTiO_3$ and (b) $Ba_{0.9}Zn_{0.1}Ti_{0.9}Mn_{0.1}O_3$ ceramic samples.

Raman spectroscopy is a highly sensitive technique to probe the structural changes in comparison with x-ray

diffraction. The Raman spectra of the $BaTiO_3$ (BTO) and $Ba_{0.9}Zn_{0.1}Ti_{0.9}Mn_{0.1}O_3$ are shown in Fig. 3. For BTO, peaks around 183, 261, 304, 517, and 715 cm^{-1} are observed. The above peaks clearly indicate that BTO is in the tetragonal phase.[18] The peak around 183 cm^{-1} is assigned to a longitudinal optical mode with A_1 (LO) symmetry.[18] Bands observed around 261 cm^{-1} and 517 cm^{-1} are assigned to the transverse optical modes with A_1 (TO) and E (TO) symmetry respectively.[18] A peak located around 304 cm^{-1} is assigned to B_1 mode and this mode indicates an asymmetry within the TiO_6 octahedra of BTO on a local scale.[19] The peak observed around 715 cm^{-1} is assigned to a longitudinal optical mode with A_1 (LO) symmetry.[18] In the case of $Ba_{0.9}Zn_{0.1}Ti_{0.9}Mn_{0.1}O_3$, peaks around 154, 218, 395, 411, 480, 636, and 713 cm^{-1} are observed. Peaks located around 154, 218, 395, 411, 480, and 636 cm^{-1} are Raman peaks of BTO in the hexagonal phase.[20] It is clearly revealed that $Ba_{0.9}Zn_{0.1}Ti_{0.9}Mn_{0.1}O_3$ is in the hexagonal phase. Peaks near 154, 218, and 411 cm^{-1} are assigned to E_{1g} symmetry.[20] Peaks around 395 cm^{-1} and 480 cm^{-1} are assigned to E_{2g} mode. The mode located around 636 cm^{-1} is assigned to A_{1g} symmetry.[20] However, the mode observed near 713 cm^{-1} is not associated with the hexagonal phase of BTO.[16] This peak is also not a blue shift of the peak (715 cm^{-1}) of the tetragonal phase, but a vibrational mode associated with boundary layers of hexagonal crystals continuing with tetragonal crystals.[16]

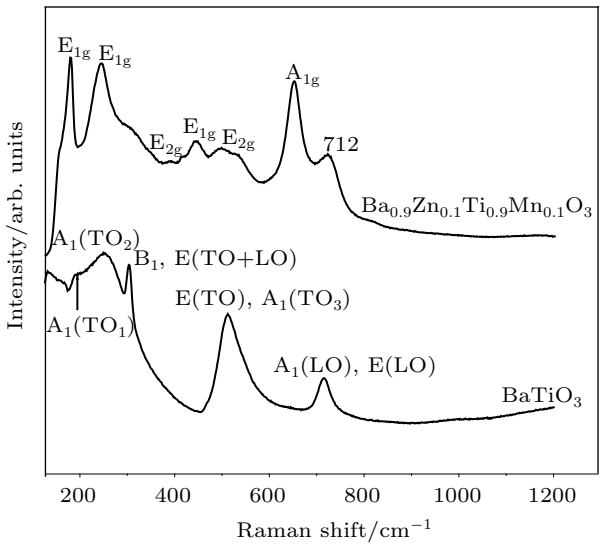


Fig. 3. The Raman scattering spectra of samples $BaTiO_3$ and $Ba_{0.9}Zn_{0.1}Ti_{0.9}Mn_{0.1}O_3$.

Figure 4 shows energy dispersive x-ray spectrum of $Ba_{0.9}Zn_{0.1}Ti_{0.9}Mn_{0.1}O_3$ ceramic. The EDX measurement shows very fewer traces of Zn in the co-doped BTO. This may be due to the fact that Zn loss has occurred during high temperature calcination and sintering as boiling temperature of Zn is around 900 °C.[21]

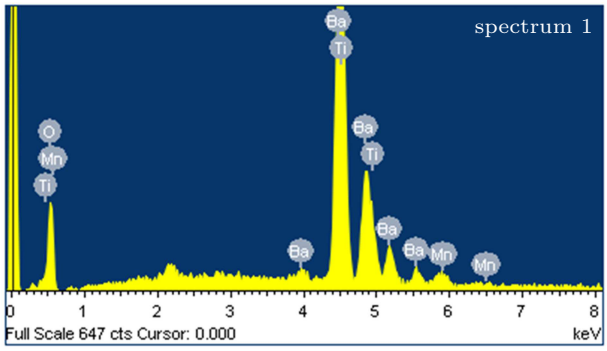


Fig. 4. (color online) The energy dispersive x-ray spectrum of $Ba_{0.9}Zn_{0.1}Ti_{0.9}Mn_{0.1}O_3$ ceramic.

In order to observe the oxidation state of the metal ions in the sintered sample, XPS studies are performed. Figure 5(a) shows the survey scan spectra of $Ba_{0.9}Zn_{0.1}Ti_{0.9}Mn_{0.1}O_3$ sintered ceramic sample. From the survey scan, it is observed that the elemental composition of the sintered sample $Ba_{0.9}Zn_{0.1}Ti_{0.9}Mn_{0.1}O_3$ is the same as the main elements of the composition. Besides the lines of the main elements such as barium, titanium, manganese, zinc, and oxygen, carbon is also detected from this spectrum. However, the intensities of the peaks related to Zn are very low, which indicates the low concentration of Zn in the composition. XPS spectrum of Zn in the composition $Ba_{0.9}Zn_{0.1}Ti_{0.9}Mn_{0.1}O_3$ is shown in Fig. 5(b). Peaks observed near 1021 eV and 1045 eV are corresponding to Zn $2p_{3/2}$ and Zn $2p_{1/2}$ states, respectively.[22] It indicates that Zn is in the +2 state.[23] It is noted that the oxidation state of Ba is also the +2 state.[12] It may also be noted that Zn is in the same oxidation state as Ba. Hence, Zn maintains its oxidation state even after in BTO. From XPS, it is observed that the valance of Zn is +2, which is the same as that of Ba, i.e., Zn is isovalent to Ba. In addition to the above, the ionic radius of Zn is less than that of Ba.[24] Hence, Zn doping at the Ba site reduces the mean A site cation radius leading to a structural distortion. In general, structural distortion favors magnetic anisotropy through its magnetostrictive effect.[25] As a result, there is more likelihood of obtaining coupling between electric and magnetic order parameters.[25] XPS spectrum of Mn ion in the composition $Ba_{0.9}Zn_{0.1}Ti_{0.9}Mn_{0.1}O_3$ is shown in Fig. 5(c). It is observed that Mn is existent in a multiple oxidation state. Peaks observed near 642 eV and 654 eV are corresponding to $2p_{1/2}$ and $2p_{3/2}$ levels of Mn^{4+} ion.[26] The peak observed near 641.8 eV can be ascribed to the Mn^{3+} state.[27] It is clearly inferred that Mn exists as Mn^{4+} and Mn^{3+} oxidation state in the ceramic composition $Ba_{0.9}Zn_{0.1}Ti_{0.9}Mn_{0.1}O_3$. It is also noted that Mn is an acceptor dopant for substitution for Ti and Mn doping leads to the formation of an oxygen vacancy in BTO. The oxygen vacancies convert the corner sharing TiO_6 octahedra into the Ti_2O_9 groups of the face-sharing octahedral thereby forming the hexagonal phase.

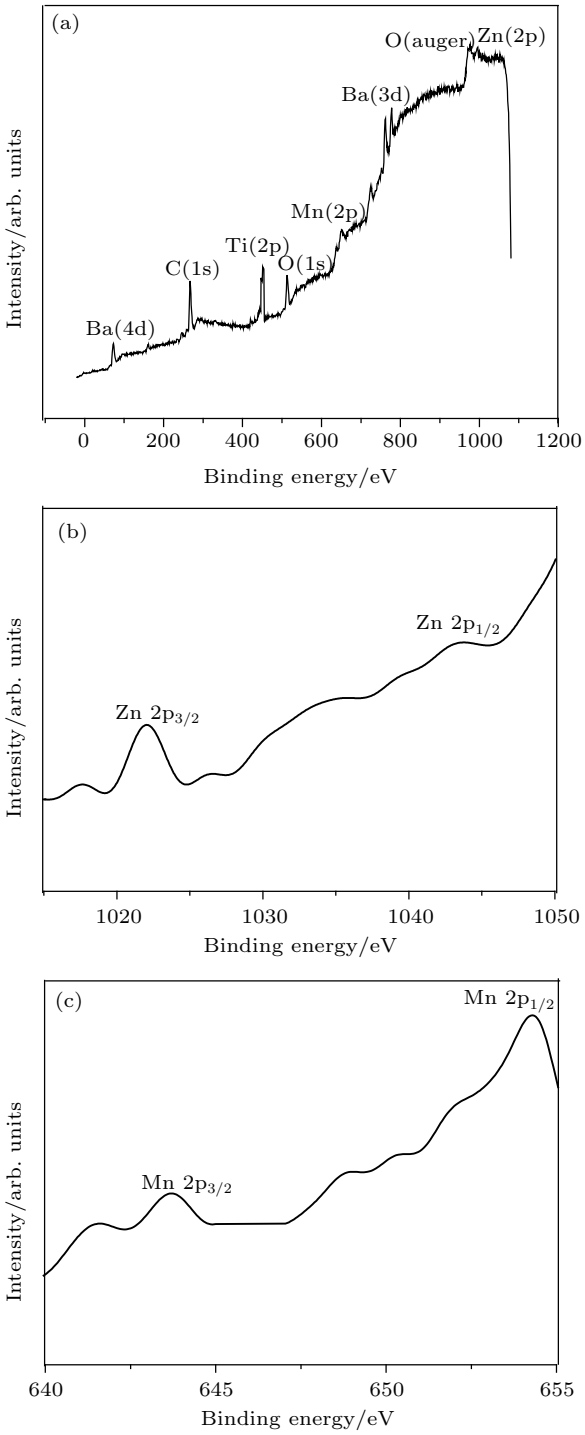


Fig. 5. (a) Survey scans spectrum of the sintered ceramic sample $Ba_{0.9}Zn_{0.1}Ti_{0.9}Mn_{0.1}O_3$; XPS spectra of (b) Zn and (c) Mn in the sintered ceramic composition $Ba_{0.9}Zn_{0.1}Ti_{0.9}Mn_{0.1}O_3$.

Figure 6(a) shows the room temperature magnetic hysteresis loops of pure BTO, $Ba_{0.94}Zn_{0.06}Ti_{0.94}Mn_{0.06}O_3$, and $Ba_{0.9}Zn_{0.1}Ti_{0.9}Mn_{0.1}O_3$. BTO ceramic shows diamagnetic-type behavior. Double loop type behavior is observed in $Ba_{0.9}Zn_{0.1}Ti_{0.9}Mn_{0.1}O_3$. Hence, magnetization does not become saturated even in a field of 2 T. Further high field cannot be applied due to the limitation of our instrument. In the case of $Ba_{0.9}Zn_{0.1}Ti_{0.9}Mn_{0.1}O_3$, the hysteresis loop is narrowed near $H = 0$, which is very different from that of ferromagnets. In the case of ferromagnets, hysteresis loops are widened near the origin. $Ba_{0.9}Zn_{0.1}Ti_{0.9}Mn_{0.1}O_3$ ceramic exhibits a loop that is divided into two sub-loops, one shifts toward positive fields and the other toward the negative fields, rather than a single shifted hysteresis loop as that of a typical ferromagnetic sample. A similar kind of magnetic hysteresis loop has also been observed in bilayer systems[28] consisting of ferromagnetic and antiferromagnetic films cooled or grown below the antiferromagnetic Neel temperature, in the presence of a static magnetic field. In general, double loop type phenomena are observed due to exchange bias between ferromagnetic and antiferromagnetic interfaces.[29] From XRD, we have not observed any impurity phase for the composition $Ba_{0.9}Zn_{0.1}Ti_{0.9}Mn_{0.1}O_3$. Hence, the magnetic signal, which we have obtained from the co-doped BTO, is intrinsic in nature. The *M–H* measurement of the composition $Ba_{0.9}Zn_{0.1}Ti_{0.9}Mn_{0.1}O_3$ is carried out at 10 K to reveal its magnetic behavior further. It is shown in the inset of Fig. 6(a). A weak ferromagnetic type of hysteresis loop is clearly observed at 10 K. We carry out the magnetic measurements of another co-doped composition $Ba_{0.94}Zn_{0.06}Ti_{0.94}Mn_{0.06}O_3$, and a similar type of magnetic behavior is observed. Hence, it is inferred from the observation that the magnetism depends on the doping concentration.

In order to know the details about the magnetic properties of the highest magnetized composition, i.e., $Ba_{0.9}Zn_{0.1}Ti_{0.9}Mn_{0.1}O_3$, the temperature dependence of magnetization (*M–T*) is investigated. The *M–T* measurements are carried out in the zero-field-cooled (ZFC) and field-cooled (FC) modes at an applied field of 10 kOe. Figure 6(b) shows the temperature dependence of magnetization of the sample $Ba_{0.9}Zn_{0.1}Ti_{0.9}Mn_{0.1}O_3$ under an applied field of 10 kOe. The *M–T* curve shows concave temperature dependence. The ZFC and FC curve of the sample nearly coincided well in the measured temperature range. Hence, spin glass or superparamagnetic behavior can be ruled out.[30] The magnetization value is increased sharply below 50 K. Figure 6(c) shows the curve of inverse susceptibility ($1/\chi$) as a function of temperature for the ceramic composition $Ba_{0.9}Zn_{0.1}Ti_{0.9}Mn_{0.1}O_3$. It is observed from Fig. 6(c) that the temperature-dependent inverse susceptibility curve does not follow the Curie–Weiss dependence for pure paramagnetic, ferromagnetic or antiferromagnetic properties. An ideal paramagnet has a linear relationship between inverse susceptibility and temperature that intersects at zero.[31] However, the ferromagnetic material exhibits a downward deviation, while an antiferromagnetic material exhibits an upward deviation. In all the cases, the *M–T* curve in high temperature is linear because the thermal energy is greater than the energy of the magnetic interaction. However, in our case, the temperature-dependant inverse susceptibility curve deviates slightly from *a* straight line at high temperature and near low temperature the curve deviates down-

ward. Hence, it indicates that the collective behavior of different types of exchange interactions such as ferromagnetic and antiferromagnetic exchange interactions are present in the composition $Ba_{0.9}Zn_{0.1}Ti_{0.9}Mn_{0.1}O_3$.

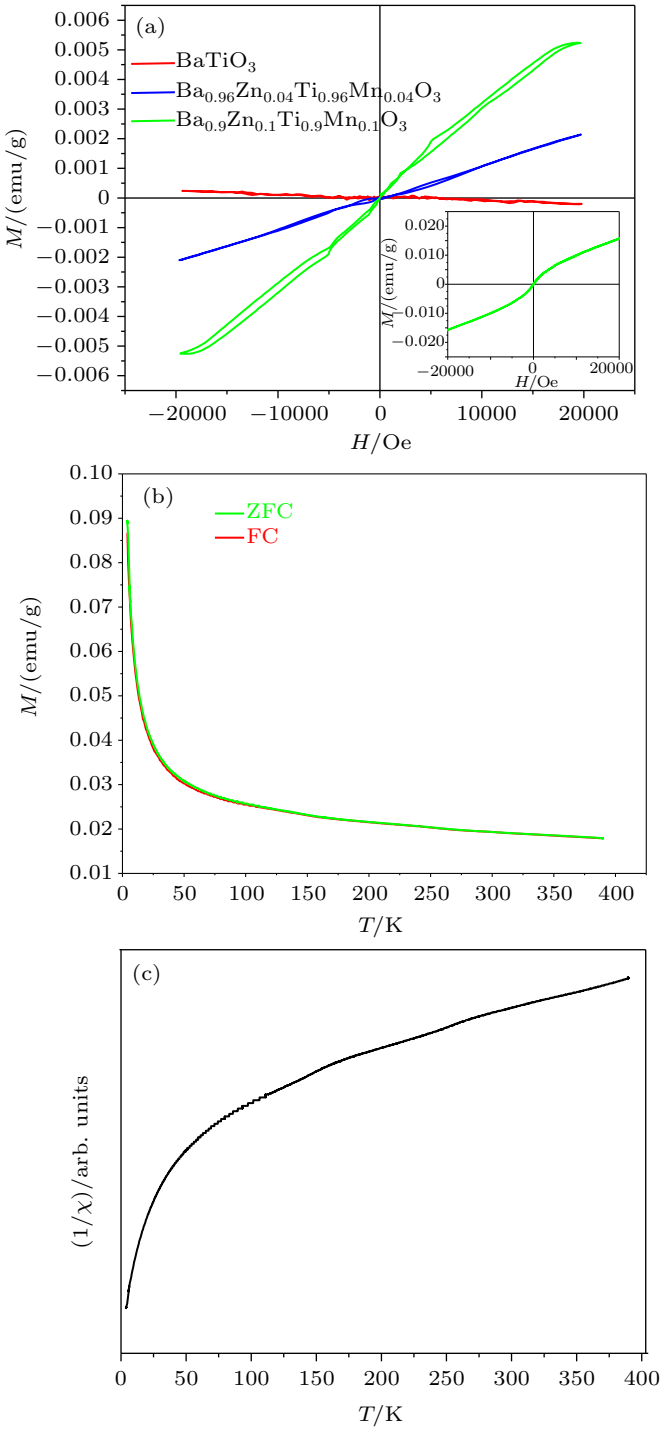


Fig. 6. (color online) (a) Room temperature magnetic hysteresis loops of $BaTiO_3$, $Ba_{0.96}Zn_{0.04}Ti_{0.96}Mn_{0.04}O_3$, and $Ba_{0.9}Zn_{0.1}Ti_{0.9}Mn_{0.1}O_3$ ceramic samples and the inset shows the M–H loop of $Ba_{0.9}Zn_{0.1}Ti_{0.9}Mn_{0.1}O_3$ at 10 K, (b) temperature dependences of magnetization in field cooled (FC) and zero field cooled (ZFC) conditions for $Ba_{0.9}Zn_{0.1}Ti_{0.9}Mn_{0.1}O_3$ ceramic, (c) $1/\chi \sim T$ curve for $Ba_{0.9}Zn_{0.1}Ti_{0.9}Mn_{0.1}O_3$ ceramic sample.

It is known that the ionic radii of Ti^{4+} and Ti^{3+} are 0.605 Å and 0.67 Å[24] respectively, and ion radii of Mn^{3+} (low spin/high spin) and Mn^{4+} are 0.58 Å/0.65 Å and 0.54 Å[24] respectively, which are comparable to the ion radius of Ti. In addition to the above, the oxidation state of the Mn ion in the composition $Ba_{0.9}Zn_{0.1}Ti_{0.9}Mn_{0.1}O_3$ is also observed to be states of Mn^{3+} and Mn^{4+} (as per the XPS measurement in Fig. 5(c)). Hence, it is evident that Mn^{3+} and Mn^{4+} ions exist in our sample. As Mn^{3+} and Mn^{4+}ions coexist in our sample, exchange interactions of Mn^{3+}–Mn^{4+}, Mn^{3+}–Mn^{3+}, and Mn^{4+}–Mn^{4+} are possible. Among these, the Mn^{3+}–Mn^{4+} exchange interaction is ferromagnetic while other exchange interactions are antiferromagnetic.[16] Hence, the M–H loop observed for the ceramic composition $Ba_{0.9}Zn_{0.1}Ti_{0.9}Mn_{0.1}O_3$ near room temperature is expected to be due to the simultaneous occurrence of ferromagnetic and antiferromagnetic exchange interactions.

P–E curves of BTO, $Ba_{0.96}Zn_{0.04}Ti_{0.96}Mn_{0.04}O_3$, and $Ba_{0.9}Zn_{0.1}Ti_{0.9}Mn_{0.1}O_3$ ceramics at room temperature are shown in Fig. 7. The P–E loop observed for the sample $Ba_{0.9}Zn_{0.1}Ti_{0.9}Mn_{0.1}O_3$ decreases noticeably compared with that for BTO. The saturation polarization values of BTO, $Ba_{0.96}Zn_{0.04}Ti_{0.96}Mn_{0.04}O_3$, and $Ba_{0.9}Zn_{0.1}Ti_{0.9}Mn_{0.1}O_3$ are 17.3 μC/cm^2, 1.18 μC/cm^2, and 0.33 μC/cm^2 respectively. Coercive fields for the BTO, $Ba_{0.96}Zn_{0.04}Ti_{0.96}Mn_{0.04}O_3$, and $Ba_{0.9}Zn_{0.1}Ti_{0.9}Mn_{0.1}O_3$ are 2.2 kV/cm, 4.2 kV/cm, and 5.5 kV/cm respectively. The above observation indicates that the coercive field for co-doped BTO remains high, despite a sharp reduction in the saturation polarization value. The co-doped BTO has also shown the lossy-type ferroelectric behavior.

In general, the stability of the ferroelectric phase depends on the structural transition with additional factors like the incorporation of foreign atoms, grain size, the presence of structural imperfections such as oxygen vacancies, and dislocations.[8] In our case, the ferroelectricity in co-doped BTO decreases. This decrease of ferroelectricity may be due to the arising of the hexagonal phase, and the hexagonal phase has much poorer ferroelectric properties.[4] A similar type of observation for Fe-doped BTO has also been reported by Yu *et al.*[32]

Frequencies as well as temperature-dependent dielectric measurements are performed to reveal the dielectric response of the substitution of Zn and Mn in BTO. The dielectric constant of the compositions as a function of frequency is shown in Fig. 8(a), and the inset of Fig. 8(a) shows the frequency variations of the dielectric loss of different compositions. It is observed that dielectric constants decrease sharply with the increasing of frequency and the rate of decrease levels off in a certain frequency range. This is due to the different polarization mechanisms at different frequencies.[33] At low frequency, electron displacement polarization, ion displacement polarization, and oriental polarization contribute to the dielectric constant.[33] At high frequency, the dielectric constant just

results from the electron displacement polarization.[33] The dielectric loss also follows a similar type of trend to the dielectric constant, but the losses increase slightly with the increasing of doping ion concentration. Figure 8(b) shows the temperature dependences of the dielectric constants of samples in a temperature range from 30 °C to 170 °C at 1 kHz and the inset of Fig. 8(b) shows the temperature variations of dielectric loss for different concentrations. It is also observed that the Curie temperature as well as the maximum dielectric constant decreases with increasing the doping level. Although the Curie temperature decreases in the doped composition, it is well above room temperature. In the case of dielectric loss, it is observed that the loss is independent of temperature nearly up to 125 °C, 110 °C, and 80 °C for the BTO, $Ba_{0.96}Zn_{0.04}Ti_{0.96}Mn_{0.04}O_3$, and $Ba_{0.9}Zn_{0.1}Ti_{0.9}Mn_{0.1}O_3$ respectively and then rapidly increases with increasing the temperature. This sharp increase of dielectric loss in a high temperature range may be attributed to the increased mobility of charge carriers due to defects or vacancies in the sample.[34] The resistivities of samples are measured using an electrometer and they are observed to be 1.2×10^9 Ω·cm, 3.05×10^8 Ω·cm, and 0.51×10^8 Ω·cm for the BTO, $Ba_{0.96}Zn_{0.04}Ti_{0.96}Mn_{0.04}O_3$, and $Ba_{0.9}Zn_{0.1}Ti_{0.9}Mn_{0.1}O_3$ respectively. It is observed that the resistivity of the sample decreases with increasing the doping ion concentration.

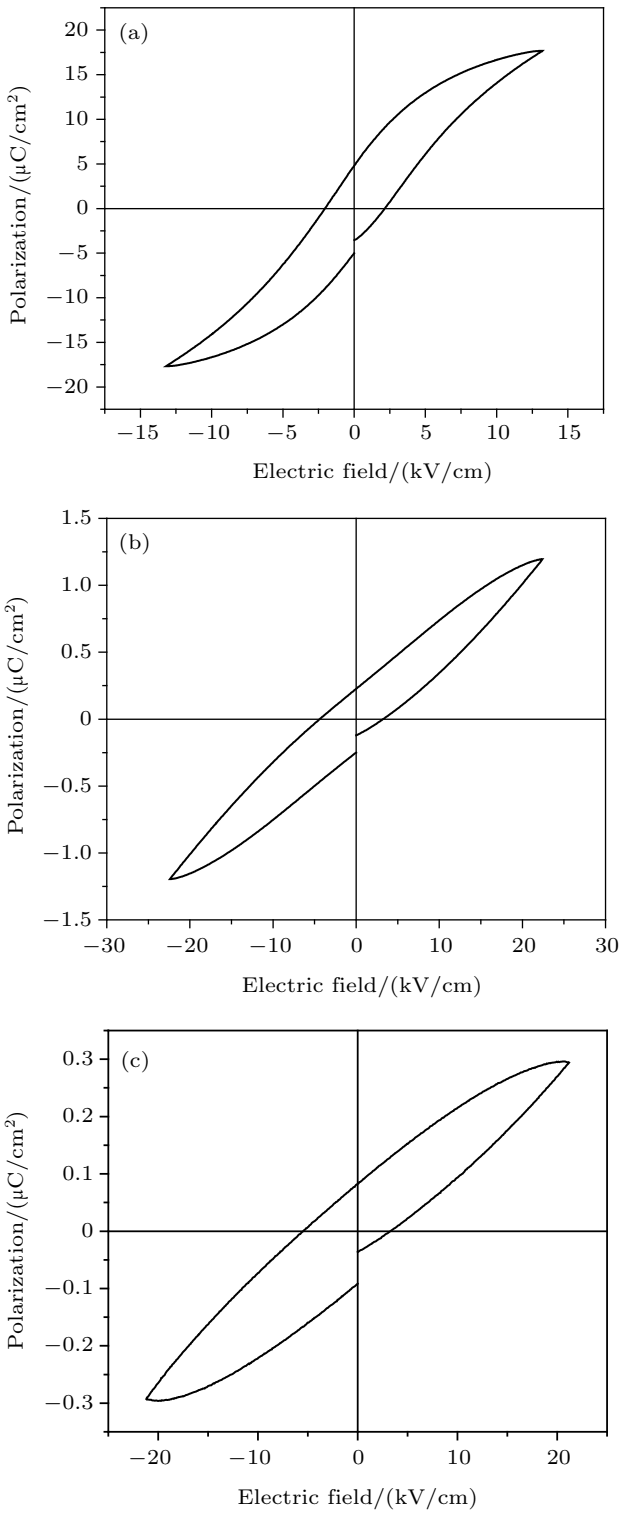


Fig. 7. The room temperature *P*–*E* loops of (a) $BaTiO_3$, (b) $Ba_{0.96}Zn_{0.04}Ti_{0.96}Mn_{0.04}O_3$, and (c) $Ba_{0.9}Zn_{0.1}Ti_{0.9}Mn_{0.1}O_3$ ceramic samples.

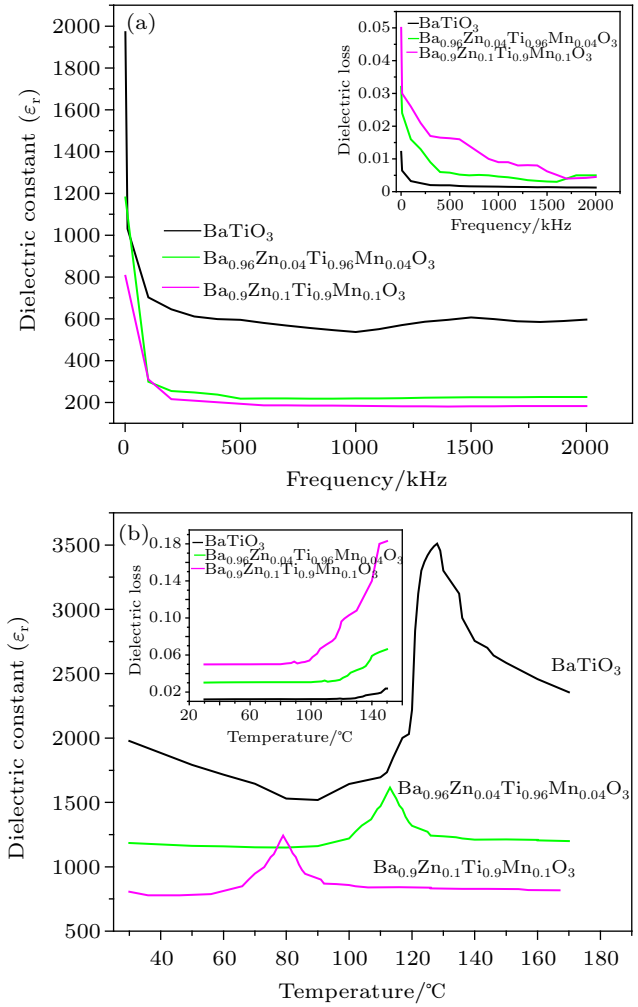


Fig. 8. (color online) (a) Dielectric constants versus frequency and the inset shows the frequency variations of dielectric loss of different compositions and (b) the temperature dependences of the dielectric constants of samples in a temperature range from 30 °C to 170 °C at 1 kHz and the inset shows the temperature variations of dielectric loss of different concentrations.

It should also be noted that Zn is substituted for Ba and ion radius of Zn is lower than that of Ba.[24] Hence, the substitution of Zn for Ba reduces the mean A site cation radius.[35] It may be likely to reduce the value of T_c. In addition to the above, the decrease in Curie temperature may be due to the formation of oxygen vacancies.[34] As Mn is an acceptor type of dopant in BTO[36] and substitution of Mn for Ti leads to the formation of an oxygen vacancy.[35] Oxygen vacancies in combination with acceptor impurities give rise to the local deformation of perovskite unit cells, leading to a decrease in Curie temperature.[34]

4. Conclusion

In this study, a clear signature of room temperature multiferroicity is observed for the typical composition $Ba_{0.9}Zn_{0.1}Ti_{0.9}Mn_{0.1}O_3$. Peculiar magnetic behaviors are shown by all the co-doped ceramic compositions in which magnetic hysteresis loops are narrowed near the origin. Such a magnetic effect may be attributed to the coexistence of antiferromagnetic and ferromagnetic exchange interactions between Mn^{3+} and Mn^{4+} ions. Although the ferroelectric polarization decreases in co-doped compositions, the ferroelectricity shown by co-doped compositions is present well above room temperature. This type of ferroelectric behavior observed in co-doped BTO is due to the presence of a hexagonal structural phase. This work could be helpful in shedding light on exploring the multiferroicity effect in prominent ferroelectric materials like barium titanate.

Acknowledgment

The authors of this paper are grateful to Mr. S. Choudhury of IOP, Bhubaneswar for his help in carrying out XPS measurements and to CIF, IIT-Guwahati and CRF, IIT-Kharagpur for magnetic measurements. We also thank CRF, IIT-Kharagpur for EDS study and IMMT, Bhubaneswar for the Raman study.

References

[1] Salonitis K, Pandremenos J, Paralikas J and Chryssolouris G 2010 *Int. J. Adv. Manuf. Tech.* **49** 803
[2] Gong G, Fang Y, Zerihun G, Yin C, Huang S and Yuan S 2014 *J. Appl. Phys.* **115** 243902
[3] Maier R, Cohn J L, Neumeier J J and Bendersky L A 2001 *Appl. Phys. Lett.* **78** 2536
[4] Du G P, Hu Z J, Han Q F, Qin X M and Shi W Z 2010 *J. Alloys Compds.* **492** L79
[5] Shao D F, Yang J, Jian H B, Zhu X B and Sun Y P 2013 *J. Appl. Phys.* **113** 063902
[6] Huang F, Jiang Z, Lu X, Ti R, Wu H, Yi K and Zhu J 2014 *Appl. Phys. Lett.* **105** 022904
[7] Vijatović M M, Bobić J D and Stojanović B D 2008 *Sci. Sint.* **40** 235
[8] Zhao Z, Buscaglia V, Viviani M, Buscaglia M T, Mitoseriu L, Testino A, Nygren M, Johnsson M and Nanni P 2004 *Phys. Rev. B* **70** 024107
[9] Benedek N A, Mulder A T and Fennie C J 2012 *J. Solid State Chem.* **195** 11
[10] Dang N V, Thanh T D, Hong L V, Lam V D and Phan T L 2011 *J. Appl. Phys.* **110** 043914
[11] Gruber C, Bedolla-Velazquez P O, Redinger J, Mohn P and Marsman M 2012 *Europhys. Lett.* **97** 67008
[12] Das S K, Rout P P, Pradhan S K and Roul B K 2012 *J. Adv. Ceram.* **1** 241
[13] Nakayama H and Yoshida H K 2001 *Jpn. J. Appl. Phys.* **40** L1355
[14] Mangalam R V K, Ray N, Waghmare U V, Sundaresan A and Rao C N R 2009 *Solid State Commun.* **49** 1
[15] Apostolova I N, Apostolov A T, Bahoosh S G and Wesselinowa J M 2013 *J. Appl. Phys.* **113** 203904
[16] Phan T L, Zhang P, Grinting D, Yu S C, Nghia N X, Dang N V and Lam V D 2012 *J. Appl. Phys.* **112** 013909
[17] Roul B K 2001 *J. Supercond.* **14** 529
[18] Venkateswaran U D, Naik V M and Naik R 1998 *Phys. Rev. B* **58** 14256
[19] Deng Z, Dai Y, Chen W, Pei X and Liao J 2010 *Nanoscale Res. Lett.* **5** 1217
[20] Yamaguchi H, Uwe H, Sakudo T and Sawaguchi E 1987 *J. Phys. Soc. Jpn.* **56** 589
[21] Zheng H, Li L, Xu Z, Weng W, Han G Ma N and Du P 2013 *J. Appl. Phys.* **113** 044101
[22] Ievtushenko A, Khyzhun O, Shtepliuk I, Tkach V, Lazorenko V and Lashkarev G 2013 *Acta Phys. Polon. A* **124** 858
[23] Biesingera M C, Laua L W M, Gerson A R and Smart R S C 2010 *Appl. Surf. Sci.* **257** 887
[24] Shannon R D and Prewitt C T 1969 *Acta Cryst.* **B25** 925
[25] Zheng H, Wang J, Lofland S E, Ma Z, Mohaddes-Ardabili L, Zhao T, Salamanca-Riba L, Shinde S R, Ogale S B, Bai F, Viehland D, Jia Y, Schlom D G, Wuttig M, Roytburd A and Ramesh R 2004 *Science* **303** 661
[26] Miyakoshi A, Ueno A and Ichikawa M 2001 *Appl. Catal. A* **219** 249
[27] Xuesong L, Jiqing L, Kun Q, Weixin H and Mengfei L 2009 *J. Rare Earths* **27** 418
[28] Zhao H W, Wang W N, Wang Y J, Zhan W S and Xiao J Q 2002 *J. Appl. Phys.* **91** 6893
[29] Brück S, Sort J, Baltz V, Suriñach S, Muñoz J S and Dieny B 2005 *Adv. Mater.* **17** 2978
[30] Wei X K, Su Y, Sui Y, Zhou Z, Yao Y, Jin C and Yu R 2013 *Appl. Phys. Let.* **102** 242910
[31] Maurer J A 2003 "I: Structure-Function Analysis of the Mechanosensitive Channel of Large Conductance. II. Design of Novel Magnetic Materials using Crystal Engineering", Ph. D Thesis, California Institute of Technology, USA
[32] Yu Q S, Wang L, Yu L, Hua L G, Qiang W Y and Nan C 2010 *Trans. Nonferrous Met. Soc. China* **20** 1911
[33] Das S K, Mishra R N and Roul B K 2014 *Appl. Phys. A* **116** 1897
[34] Jha P A and Jha A K 2012 *J. Alloys Compd.* **513** 580
[35] Ferrarelli M C, Tan C C and Sinclair D C 2011 *J. Mater. Chem.* **21** 6292
[36] Wei X K, Zhang Q H, Li F Y, Jin C Q and Yu R C 2010 *J. Alloys Compd.* **508** 486